BRIEF ARTICLE

Improved Debulking of Peritoneal Tumor Implants by Near-Infrared Fluorescent Nanobody Image Guidance in an Experimental Mouse Model

Pieterjan Debie,[1] Marian Vanhoeij,[2] Natalie Poortmans,[2] Janik Puttemans,[1] Kris Gillis,[1,3] Nick Devoogdt,[1] Tony Lahoutte,[1,4] Sophie Hernot[1]

[1]Laboratory for In vivo Cellular and Molecular Imaging, ICMI-BEFY, Vrije Universiteit Brussel, Laabeeklaan 103, 1090, Jette, Brussels, Belgium
[2]Department of Oncological Surgery, UZ Brussel, Brussels, Belgium
[3]Department of Cardiology, UZ Brussel, Brussels, Belgium
[4]Department of Nuclear Medicine, UZBrussel, Brussels, Belgium

Abstract

Purpose: Debulking followed by combination chemotherapy is currently regarded as the most effective treatment for advanced ovarian cancer. Prognosis depends drastically on the degree of debulking. Accordingly, near-infrared (NIR) fluorescence imaging has been proposed to revolutionize cancer surgery by acting as a sensitive, specific, and real-time tool enabling visualization of cancer lesions. We have previously developed a NIR-labeled nanobody that allows fast, specific, and high-contrast imaging of HER2-positive tumors. In this study, we applied this tracer during fluorescence-guided surgery in a mouse model and investigated the effect on surgical efficiency.
Procedures: 0.5×10^6 SKOV3.IP1-Luc+ cells were inoculated intraperitoneally in athymic mice and were allowed to grow for 30 days. Two nanomoles of IRDye800CW-anti-HER2 nanobody was injected intravenously. After 1h30, mice were killed, randomized in two groups, and subjected to surgery. In the first animal group ($n = 7$), lesions were removed by a conventional surgical protocol, followed by excision of remaining fluorescent tissue using a NIR camera. The second group of mice ($n = 6$) underwent directly fluorescence-guided surgery. Bioluminescence imaging was performed before and after surgery. Resected tissue was categorized as visualized during conventional surgery or not, fluorescent or not, and bioluminescent positive or negative.
Results: Fluorescence imaging allowed clear visualization of tumor nodules within the abdomen, up to submillimeter-sized lesions. Fluorescence guidance resulted in significantly reduced residual tumor as compared to conventional surgery. Moreover, sensitivity increased from 59.3 to 99.0 %, and the percentage of false positive lesions detected decreased from 19.6 to 7.1 %.
Conclusions: This study demonstrates the advantage of intraoperative fluorescence imaging using nanobody-based tracers on the efficiency of debulking surgery.

Key words: Nanobody, Near-infrared fluorescent tracer, Targeted tracer, Ovarian cancer, Fluorescence-guided surgery, Intraoperative imaging

---

Pieterjan Debie and Marian Vanhoeij contributed equally.

Correspondence to: Pieterjan Debie; e-mail: pieterjan.debie91@gmail.com

Introduction

To date, ovarian cancer remains the deadliest gynecological disease in the western world [1, 2]. Due to late presentation of clear symptoms, disease is often diagnosed in an

advanced stage, where metastasis to the peritoneal cavity has already taken place [3, 4]. The standard treatment consists of surgical debulking followed by combination chemotherapy. Notably, overall survival is greatly impacted by the efficiency of the debulking surgery, with clear improvements seen for complete debulking over (sub-)optimal debulking [5–8]. However, due to the highly disseminated nature of late stage ovarian cancer, such complete debulking is a difficult, time-consuming, and intensive procedure [5, 7, 9].

There is strong evidence that intraoperative guidance, by which tissues of interest are marked using a fluorescent contrast agent, can lead to a more precise and more thorough resection of tumor tissue, with ultimately reduced mortality and morbidity rates [7, 10]. The feasibility and benefit of fluorescence-guided debulking surgery to detect an increased number of tumor lesions has been demonstrated by van Dam *et al.* [11] and Hoogstins *et al.* [12] using fluorescently labeled folate. Since then, several additional clinical trials have investigated the application of targeted fluorescent tracers in the wide field of surgical oncology and showed that an increase in tumor-to-background signal ratio has a beneficial effect on the sensitivity of tumor detection [13–15]. These tracers are often based on antibodies that are already being used for immunotherapy [10].

While such monoclonal antibodies bind their targets with high affinity, their long biological half-life does entail certain disadvantages regarding specificity and the time necessary to attain sufficient contrast [16]. Therefore, nanobody-based tracers are believed to have more attractive characteristics [17]. Nanobodies are the antigen-binding domains of heavy chain-only antibodies found in all members of the Camelid family [18]. As demonstrated by our group and others, their unique attributes in terms of stability, specificity, and pharmacokinetics enable rapid and high-contrast molecular imaging, both for nuclear and optical imaging applications [19–25].

In this study, an anti-HER2 nanobody, labeled site specifically with the near-infrared (NIR) dye IRDye800CW, and previously validated in terms of biodistribution and specific tumor targeting [20], was used to assess the potential of nanobody-based NIR tracers for fluorescence-guided surgery in a mouse model with disseminated peritoneal tumor lesions, mimicking late stage ovarian cancer [20].

Methods

Tracer Preparation

The preparation and characterization of the anti-HER2 NIR-nanobody 2Rs15dCys-IRDye800CW has been described previously [20]. Briefly, after reduction of 2 mg cysteine-tagged nanobody 2Rs15d with × 180 molar excess of 2-mercaptoethylamine (2-MEA, Acros Organics), the nanobody was incubated for 2 h at 37 °C with × 5 molar excess maleimide-activated IRDye800CW (LI-COR) at pH 6. The NIR-labeled nanobody was subsequently purified by size-exclusion chromatography, and dye-to-protein ratio was determined through UV-VIS spectrophotometry (Nanodrop 2000, Thermo Fisher). A mean of 0.6–0.7 IRDye800CW molecules per nanobody was obtained.

Mouse Model of Intraperitoneally Disseminated Ovarian Cancer

HER2-expressing SKOV3.ip1 Fluc$^+$ cells were kindly provided by Prof. Marc Bracke (UGent, Belgium). These human ovarian cancer cells have been transfected with a pFL4.76 plasmid for luciferase expression and selected for improved intraperitoneal growth [26]. The cells were cultured at 37 °C in 95 % air/5 % CO$_2$ in DMEM medium (Gibco, Invitrogen) with 10 % fetal bovine serum (FBS, Merck Millipore) and antibiotics (penicillin (89 units/ml)/ streptomycin (89 µg/ml), Gibco, Invitrogen). Female Crl:NU-Foxn1^{nu} mice were obtained from Charles River (France) and injected intraperitoneally with 0.5×10^6 SKOV3.ip1 Fluc$^+$ cells. Tumors were allowed to grow for 30 days.

Experimental Setup

A schematic overview of the experimental setup is provided in Fig. 1. The aim of the experiment was to generate a proof-of-concept of the utility of nanobody-based tracers in image-guided surgery. All animal study protocols were approved by the Ethical Committee for Animal Experiments of the Vrije Universiteit Brussel. The surgical procedures were performed by a team of two trained oncologic surgeons.

2Rs15dCys-IRDye800CW (2 nmol based on dye concentration) was injected intravenously *via* the tail vein, 90 min before the animals were killed for further surgical procedures. In addition, 10 min before killing, 150 mg/kg D-luciferin (Promega) was injected intraperitoneally enabling bioluminescence imaging (BLI) (Optima, Biospace; 5 min per acquisition) of the exposed abdominal region just before surgery.

Mice were allocated randomly to two experimental groups. In the first group ($n = 7$), complete debulking was performed according to a conventional surgical protocol based on systematic visual inspection under bright light and palpation, followed by excision of remaining fluorescent tissue as detected with the NIR fluorescent camera FluoBeam800 (Fluoptics) (exposure time per frame 50 ms). The second group of mice ($n = 6$) underwent surgical debulking, guided directly by continuous video-rate fluorescence imaging (Fluobeam800, Fluoptics, exposure time per frame 50 ms). Finally, the operated animals were imaged again using BLI, as were the resected tissues to assess their tumor status. The latter were then categorized as suspected of malignancy during conventional surgery or not, fluorescent or not, and bioluminescent positive or negative, to
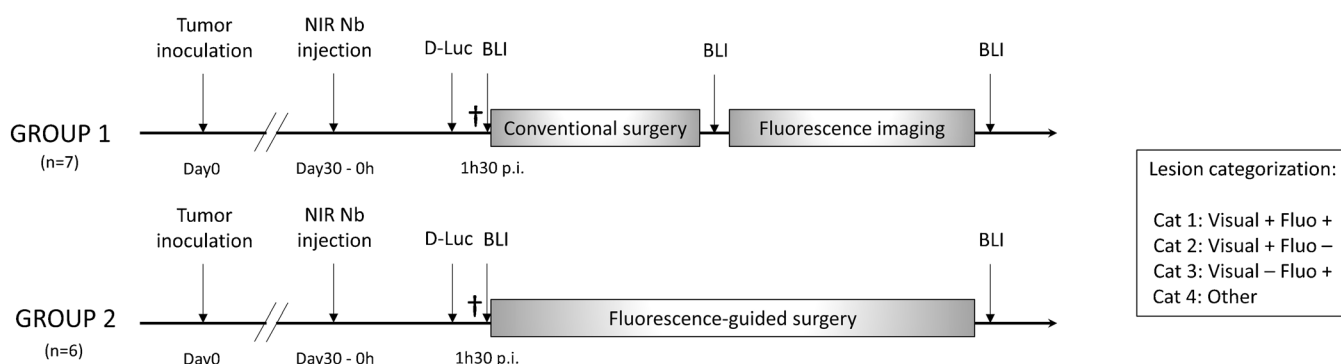
Fig. 1. Schematic representation of experimental setup. Mice bearing intraperitoneal tumor lesions were injected intravenously with IRDye800CW-labeled anti-HER2 nanobody. After 90 min, mice were euthanized and subjected to surgery. In group 1, lesions were removed by a conventional surgical protocol, followed by excision of remaining fluorescent tissue using a NIR fluorescent camera. Group 2 underwent directly fluorescence-guided surgery. Bioluminescence imaging was performed before and after each surgery. Resected tissue was categorized as visualized during conventional surgery or not, fluorescent or not, and bioluminescent positive or negative.

enable calculation of true positive and false negative rates, and the percentage of false positive lesions. Resected tissue samples which were not considered as tumor tissue, neither based on visual inspection or fluorescence imaging (*e.g.*, kidneys), were placed under category 4 ("Other").

From an additional set of tumor-bearing animals ($n = 3$) injected with 2 nmol NIR nanobody, one observer quantified the fluorescence intensity and 2D surface area of resected tumor lesions after acquisition with the FluoBeam800 (acquisition time 30 ms) in Image J, as well as the non-specific fluorescence signal of relevant intraperitoneal organs and tissues, including liver, muscle, abdominal fat, uterus, ovaries, pancreas, intestines, and spleen.

Data Analysis and Statistical Analysis

Based on the BLI read-out of the resected tissues, true positive rates (TPR or sensitivity) and false negative rates (100-TPR) were calculated. In addition, the percentage of false positives (%FP) resected lesions was determined by dividing the number of BLI-negative resected lesions by the total number of resected lesions × 100.

For the quantification of the percentage of BLI signal remaining in the animal after surgery, compared to before surgery, a correction factor of 0.5 % per minute elapsed after initial BLI acquisition was used to account for the natural decay of the BLI signal following intraperitoneal injection of D-luciferin [27]. Data is expressed as mean ± standard deviation. Variables were tested for homogeneity of variance by a Levene's test. Comparison between the different groups was performed by one-way ANOVA with Bonferroni correction for multiple comparisons using SPSS Statistics software (version 24.0.0, IBM). A p value $\leq$ 0.05 was considered significant.

Tumor-to-background ratios (TBR) were calculated *ex vivo* by dividing the mean fluorescent intensity of tumor lesions to the mean fluorescent intensity of peritoneal organs and tissues (excluding liver and kidneys).

Results

Intraperitoneal tumor inoculation led to the formation of numerous individual tumor implants of different sizes on peritoneal organs and tissues [26]. Debulking in mice cadavers was performed either according to a conventional surgical procedure, followed by fluorescence-aided resection, or directly guided by fluorescence. During fluorescence imaging, the kidneys had to be removed because their high non-specific signal (due to renal clearance of nanobody-based tracers) was interfering with the fluorescent signal of the tumor lesions. Thereafter, fluorescence imaging allowed clear visualization of tumor nodules within the peritoneal cavity, up to submillimeter-sized lesions (Fig. 2, Video S1 in Electronic Supplementary data).

Average duration of surgery was 20 ± 5 min for conventional surgery, 24 ± 4 min for the ensuing additional fluorescence-aided resection (group 1), and 34 ± 9 min when debulking was performed directly guided by fluorescence imaging (group 2).

Conventional surgery resulted in the resection of 143 tissue specimens for group 1; using subsequent fluorescence imaging, an additional 106 specimens were removed. True positive rates were 59.3 and 95.4 % for conventional and conventional surgery followed by fluorescence imaging, respectively. The majority of the false positive fluorescent tissues could be identified as non-specific fluorescent hot spots in stomach content, fluorescent non-invaded abdominal lymph nodes due to partial paravenous tail vein injections, and very faint and diffuse signal in some adipose
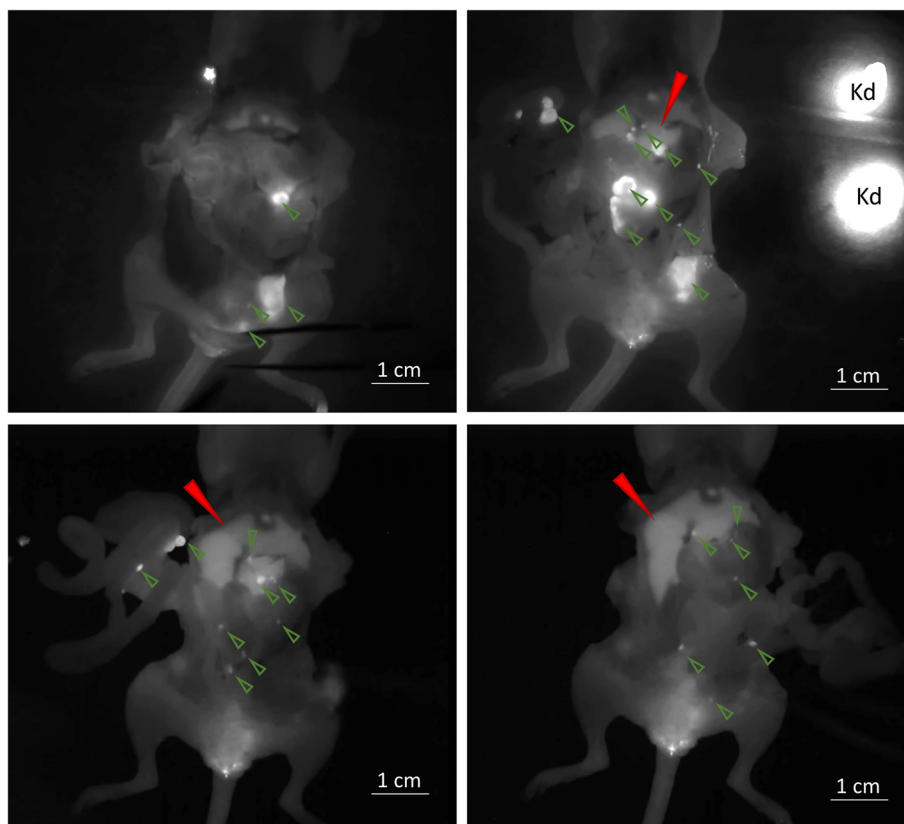
Fig. 2. Representative near-infrared fluorescent images acquired along the image-guided surgery procedure. Fluorescent signal in tumor lesions (indicated by green arrows) is clearly discernible from background signal, including signal in the liver (red arrow). Removal of the kidneys (Kd) was required because of their high fluorescent signal.

tissue near ureters, bladder, and urethra (most probably due to spilling of urine). In group 2 (fluorescence-guided surgery group), a total of 305 tissue specimens were resected, of which 93.0 % were confirmed to be tumor lesions according to BLI (true positive rate). Moreover, fluorescence guidance resulted in a decrease in the percentage of false positively detected lesions from 19.6 to 7.1 %, as compared to conventional surgery (Tables 1 and 2).

To further assess sensitivity, residual tumor tissue after surgery was measured through BLI and compared to the initial tumor burden (Fig. 3a). A significantly smaller proportion of BLI-positive residual implants were left behind in the abdomen following fluorescence imaging (be it directly fluorescence-aided debulking or

post-conventional surgery) than when debulking was performed based on visual inspection and palpation only (1.05 ± 0.58 and 0.71 ± 0.50 *vs* 2.87 ± 1.78 %, respectively, $p < 0.05$) (Fig. 3b).

The average fluorescence intensity of resected tumor lesions was plotted in function of their size in Fig. 4. A positive relationship between signal intensity and size can be observed. Fluorescent signal of most tumor lesions was higher than background signal in peritoneal organs, with an average TBR of 14.4 ± 8.5, reaching up to 42. Despite the slightly higher background signal of the liver than of other peritoneal organs and tissues (except kidneys) (Fig. 4), even small tumor lesions could be discerned on its surface (Fig. 2).

Table 1. Overview of total number of excised tissue specimens in groups 1 and 2 per category, according to "suspected of malignancy based on visual inspection under bright light and palpation, or not," fluorescently labeled or not, and BLI positive or negative (BLI-positive specimens are considered the cancerous lesions)

		Cat 1 Visual + fluo +	Cat 2 Visual + fluo −	Cat 3 Visual − fluo +	Cat 4 Other
Conventional surgery/fluorescence imaging	Total	131	12	106	–
	BLI +	114	1	70	9
Fluorescence-guided surgery	Total	302	3	7	–
	BLI +	283	2	5	3

Table 2. Calculated true positive and false negative rates for the different types of surgery, as well as the percentage of false positive lesions

	True positive rate (%)	False negative rate (%)	Percentage false positive lesions (%)
Conventional surgery	59.3	40.7	19.6
Conventional surgery/fluorescence imaging	95.4	4.6	25.7
Fluorescence-guided surgery	99.0	1.0	7.1

Discussion

The use of real-time NIR fluorescence image-guidance stands to revolutionize the surgical treatment of complex and/or locally disseminated cancers [10, 28]. More precise and more efficient intraoperative detection of malignant tissue is expected to improve surgical outcome by preventing under- and overtreatment. Peritoneal carcinomatosis is a cancer type highly amendable for fluorescence-guided surgery [13], as prognosis is greatly dependent on the amount of residual tumor after debulking. In the present study, a mouse model emulating the disease state of intraperitoneally disseminated ovarian cancer was used [26]. The model is also representative for peritoneal metastasized cancer from other origins, *e.g.*, gastrointestinal cancer [29].

We evaluated a previously characterized specific tumor-targeting nanobody conjugated with IRDye800CW as targeted fluorescent contrast agent. A cysteine-maleimide approach was chosen for conjugation of the NIR dye to the nanobody, as this strategy has demonstrated superior pharmacokinetics to the random labeling strategy, which showed high non-specific uptake and poor tumor contrast [20]. Intravenous administration of the NIR nanobody, 90 min prior to surgery only, resulted in selective labeling and accurate visualization of even submillimeter tumor lesions during debulking surgery. As compared to the

conventional surgical procedure performed under bright light, accompanying fluorescence guidance significantly increased the number of resected lesions, and consequently, reduced the amount of residual disease, as determined using BLI as gold standard. Given the targeted nature of the tracer and its rapid clearance from blood and non-targeted tissues, specificity of detection was also significantly increased. However, anatomical referencing is still warranted to prevent resection of tissues and organs that could be falsely interpreted as fluorescent cancerous tissue due to normal pharmacokinetics and clearance *via* excretory organs of the tracer (*e.g.*, kidneys, bladder, ureter, urethra).

Analogous results in terms of significantly reduced residual disease and increased sensitivity and specificity have been reported for fluorescence-guided surgery using other targeted NIR agents in a variety of orthotopic tumor models, as well as in clinical trials [11, 12, 15, 30–35]. For both the reported peptide- and monoclonal antibody-based NIR tracers, TBR typically range from two to five at their respective optimal imaging time points, *i.e.*, a few hours and several days after injection. In our study, a mean TBR of 14.4 was obtained as soon as 90 min post-injection. This early time point is very convenient in a clinical setting, since it allows our tracer to be administered just prior to surgery. Nevertheless, for long-lasting surgery, such as debulking of
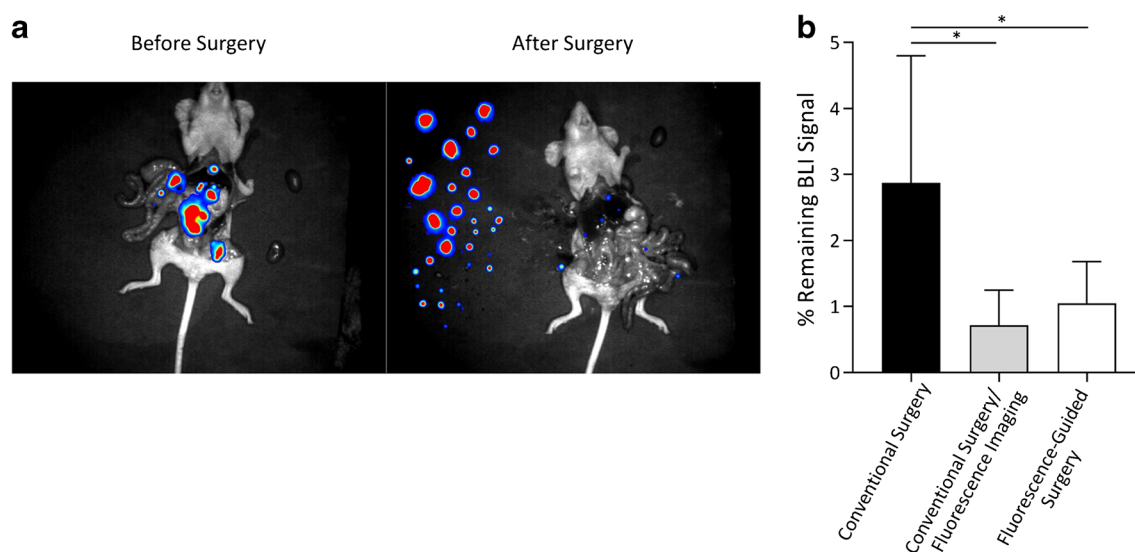

Fig. 3. a Representative BLI image of the same animal before and after image-guided surgery. *$p < 0.05$. **b** Percentage (%) remaining BLI signal after different surgical steps.
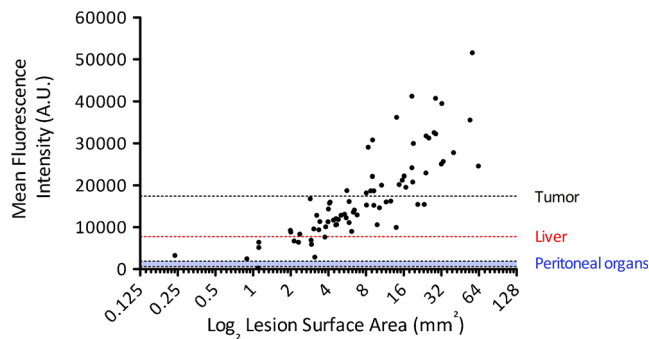
Fig. 4. Fluorescence intensity of all resected tumor lesions plotted in function of the $\log_2$ transformation of their surface area. Mean fluorescent intensity of all tumor lesions (black line) and the liver (red line) is also indicated. Background fluorescence intensity of other peritoneal organs (excluding the kidneys) is indicated as a blue-shaded area covering minimum and maximum mean fluorescence intensity of these organs.

peritoneal carcinomatosis of ovarian, colorectal or other origin, it is important that the fluorescent signal and TBR remain sufficiently high over the entire surgical procedure. We have previously demonstrated that using this NIR nanobody, specific tumor visualization was feasible for at least 24 h, since signal intensity decreases only slowly over time [20]. Inter-study comparison of TBR can, however, be largely dependent on the camera system used, the dose injected, the selected reference background, and the biomarker targeted, including its expression level. In this regard, the tumor marker HER2 was chosen as target in this study. Although HER2 overexpression in ovarian cancer is associated with a more aggressive disease, HER2 overexpression varies widely between the different subtypes of ovarian cancer [36]. Therefore, this study is more likely to serve as a proof-of-concept of the utility of the nanobodies in image-guided surgery. Pan-tumor biomarkers with high and homogenous expression only in malignant tissue, and clearly delineating the invasive front, would be more appropriate for the purpose. To this end, histopathological investigations are currently ongoing to specifically designate adequate biomarkers for image-guided surgery, in addition to $\alpha_v\beta_3$ integrin, VEGF, CAIX, uPAR, EpCAM, etc., which are often used today [37–39]. An advantage offered by the nanobody technology over peptides or small molecules is the possibility to generically design targeted molecular tracers against any biomarker of interest, with predictable in vivo properties [24, 25].

While the rapid blood clearance of nanobody tracers is considered one of their most attractive properties, the associated renal elimination causes high renal retention of the fluorescent signal [20]. This could affect the ability to detect tumor lesions in the near vicinity of the kidneys.

Given the larger dimensions and inter-organ distances in humans, as well as the relatively narrow field of view of many clinical camera systems (including laparoscopic systems), this is expected to be less of an issue in the surgical theater.

The very low hepatobiliary clearance of our tracer enabled precise identification of tumor lesions on the liver surface. Despite the use of a NIR fluorescent dye emitting around 800 nm allowing lesion detection up to a few millimeters of depth [10, 40], deeper located lesions and hidden lesions (such as micro-metastasis in lymph nodes) will remain difficult to reveal. To this end, the development of hybrid-labeled tracers, allowing both intraoperative fluorescence and nuclear detection, has been proposed [28, 41–44]. Whether this strategy is capable to further increase sensitivity remains to be demonstrated.

Conclusion

The present study demonstrates the potential of specifically targeted NIR nanobodies for highlighting intraperitoneally disseminated tumor lesions with high contrast soon after injection during fluorescence-guided surgery, resulting in increased sensitivity and specificity when compared to the conventional surgical procedure. For ovarian cancer surgery, in particular, this technology is expected to improve patients' outcome by enabling a more complete cytoreductive surgery, enhancing the effectiveness of ensuing chemotherapy, and decreasing surgical duration and associated side-effects.

Conflict of Interest

N. Devoogdt and T. Lahoutte are co-inventors on a patent relating to the compound used in this manuscript (PCT/EP2015/066430). No disclosures for other authors. No other conflicts to declare.

References

1. Ferlay J, Steliarova-Foucher E, Lortet-Tieulent J et al (2013) Cancer incidence and mortality patterns in Europe: estimates for 40 countries in 2012. Eur J Cancer 49:1374–1403
2. Bray F, Ren JS, Masuyer E, Ferlay J (2013) Global estimates of cancer prevalence for 27 sites in the adult population in 2008. Int J Cancer 132:1133–1145
3. Prat J (2014) Staging classification for cancer of the ovary, fallopian tube, and peritoneum. Int J Gynecol Obstet 124:1–5
4. Jayson GC, Kohn EC, Kitchener HC, Ledermann JA (2014) Ovarian cancer. Lancet 384:1376–1388

5. Schorge JO, McCann C, Del Carmen MG (2010) Surgical debulking of ovarian cancer: what difference does it make? Rev Obstet Gynecol 3:111–117
6. Pereira A, Pérez-Medina T, Magrina JF et al (2016) The impact of debulking surgery in patients with node-positive epithelial ovarian cancer: analysis of prognostic factors related to overall survival and progression-free survival after an extended long-term follow-up period. Surg Oncol 25:49–59
7. Lim MC, Seo S-S, Kang S et al (2012) Intraoperative image-guided surgery for ovarian cancer. Quant Imaging Med Surg 2:114–117
8. Wallace S, Kumar A, Mc M et al (2017) Efforts at maximal cytoreduction improve survival in ovarian cancer patients, even when complete gross resection is not feasible. Gynecol Oncol 145:21–26
9. Rafii A, Stoeckle E, Jean-Laurent M et al (2012) Multi-center evaluation of post-operative morbidity and mortality after optimal cytoreductive surgery for advanced ovarian cancer. PLoS One. https://doi.org/10.1371/journal.pone.0039415
10. Zhang RR, Schroeder AB, Grudzinski JJ et al (2017) Beyond the margins: real-time detection of cancer using targeted fluorophores. Nat Rev Clin Oncol. https://doi.org/10.1038/nrclinonc.2016.212
11. van Dam GM, Themelis G, Crane LMA et al (2011) Intraoperative tumor-specific fluorescence imaging in ovarian cancer by folate receptor-α targeting: first in-human results. Nat Med 17:1315–1319
12. Hoogstins CES, Tummers QRJG, Gaarenstroom KN et al (2016) A novel tumor-specific agent for intraoperative near-infrared fluorescence imaging: a translational study in healthy volunteers and patients with ovarian cancer. Clin Cancer Res 22:2929–2938
13. Tipirneni KE, Warram JM, Moore LS et al (2017) Oncologic procedures amenable to fluorescence-guided surgery. Ann Surg 266:36–47
14. Rosenthal EL, Moore LS, Tipirneni K et al (2017) Sensitivity and specificity of cetuximab-IRDye800CW to identify regional metastatic disease in head and neck cancer. Clin Cancer Res 23:4744–4752
15. Lamberts LE, Koch M, de Jong JS, et al (2016) Tumor-specific uptake of fluorescent bevacizumab-IRDye800CW microdosing in patients with primary breast cancer: a phase I feasibility study. Clin Cancer Res
16. Bannas P, Lenz A, Kunick V et al (2015) Molecular imaging of tumors with nanobodies and antibodies: timing and dosage are crucial factors for improved in vivo detection. Contrast Media Mol Imaging. https://doi.org/10.1002/cmmi.1637
17. De Vos J, Devoogdt N, Lahoutte T, Muyldermans S (2013) Camelid single-domain antibody-fragment engineering for (pre)clinical in vivo molecular imaging applications: adjusting the bullet to its target. Expert Opin Biol Ther 13:1149–1160
18. Hamers-Casterman C, Atarhouch T, Muyldermans S et al (1993) Naturally occurring antibodies devoid of light chains. Nature 363:446–448
19. Kijanka M, Warnders F-J, El Khattabi M et al (2013) Rapid optical imaging of human breast tumour xenografts using anti-HER2 VHHs site-directly conjugated to IRDye 800CW for image-guided surgery. Eur J Nucl Med Mol Imaging 40:1718–1729
20. Debie P, Van Quathem J, Hansen I et al (2017) Effect of dye and conjugation chemistry on the biodistribution profile of near-infrared-labeled nanobodies as tracers for image-guided surgery. Mol Pharm 14:1145–1153
21. Broisat A, Hernot S, Toczek J et al (2012) Nanobodies targeting mouse/human VCAM1 for the nuclear imaging of atherosclerotic lesions. Circ Res 110:927–937
22. Keyaerts M, Xavier C, Heemskerk J et al (2016) Phase I study of 68Ga-HER2-nanobody for PET/CT assessment of HER2 expression in breast carcinoma. J Nucl Med 57:27–33
23. Blykers A, Schoonooghe S, Xavier C et al (2015) PET imaging of macrophage mannose receptor-expressing macrophages in tumor stroma using 18F-radiolabeled camelid single-domain antibody fragments. J Nucl Med 56:1265–1271
24. Chakravarty R, Goel S, Cai W (2014) Nanobody: the "magic bullet" for molecular imaging? Theranostics 4:386–398
25. Steeland S, Vandenbroucke RE, Libert C (2016) Nanobodies as therapeutics: big opportunities for small antibodies. Drug Discov Today 21:1076–1113
26. De Vlieghere E, Carlier C, Ceelen W et al (2016) Data on in vivo selection of SK-OV-3 Luc ovarian cancer cells and intraperitoneal tumor formation with low inoculation numbers. Data Brief 6:542–549
27. Keyaerts M, Verschueren J, Bos TJ et al (2008) Dynamic biolumi-nescence imaging for quantitative tumour burden assessment using IV or IP administration of d-luciferin: effect on intensity, time kinetics and repeatability of photon emission. Eur J Nucl Med Mol Imaging 35:999–1007
28. Vahrmeijer AL, Hutteman M, van der Vorst JR et al (2013) Image-guided cancer surgery using near-infrared fluorescence. Nat Rev Clin Oncol 10:507–518
29. Coccolini F, Gheza F, Lotti M et al (2013) Peritoneal carcinomatosis. World J Gastroenterol 19:6979–6994
30. Harlaar NJ, Kelder W, Sarantopoulos A et al (2013) Real-time near infrared fluorescence (NIRF) intra-operative imaging in ovarian cancer using an αvβ3-integrin targeted agent. Gynecol Oncol 128:590–595
31. Handgraaf HJM, Boonstra MC, Prevoo HAJM et al (2017) Real-time near-infrared fluorescence imaging using cRGD-ZW800-1 for intra-operative visualization of multiple cancer types. Oncotarget 8:21054–21066
32. Day KE, Beck LN, Deep NL et al (2013) Fluorescently labeled therapeutic antibodies for detection of microscopic melanoma. Laryngoscope 123:2681–2689
33. Christensen A, Juhl K, Persson M et al (2017) uPAR-targeted optical near-infrared (NIR) fluorescence imaging and PET for image-guided surgery in head and neck cancer: proof-of-concept in orthotopic xenograft model. Oncotarget 8:20519–20520
34. Metildi CA, Kaushal S, Snyder CS et al (2013) Fluorescence-guided surgery of human colon cancer increases complete resection resulting in cures in an orthotopic nude mouse model. J Surg Res 179:87–93
35. Sexton K, Tichauer K, Samkoe KS et al (2013) Fluorescent affibody peptide penetration in glioma margin is superior to full antibody. PLoS One 8:1–9
36. English DP, Roque DM, Santin AD (2013) HER2 expression beyond breast cancer: therapeutic implications for gynecologic malignancies. Mol Diagn Ther 17:85–99
37. Boonstra MC, Prakash J, Van De Velde CJH et al (2015) Stromal targets for fluorescent-guided oncologic surgery. Front Oncol 5:254
38. van Oosten M, Crane LMA, Bart J et al (2011) Selecting potential targetable biomarkers for imaging purposes in colorectal cancer using target selection criteria (TASC): a novel target identification tool. Transl Oncol 4:71–82
39. Hoogstins CES, Weixler B, Boogerd LSF et al (2017) In search for optimal targets for intraoperative fluorescence imaging of peritoneal metastasis from colorectal cancer. Biomark Cancer 9:1–7
40. Weissleder R, Ntziachristos V (2003) Shedding light onto live molecular targets. Nat Med 9:123–128
41. Brouwer OR, Buckle T, Bunschoten A et al (2012) Image navigation as a means to expand the boundaries of fluorescence-guided surgery. Phys Med Biol 57:3123–3136
42. Buckle T, van Leeuwen AC, Chin PTK et al (2010) A self-assembled multimodal complex for combined pre- and intraoperative imaging of the sentinel lymph node. Nanotechnology 21:355101 (9pp)
43. van Leeuwen AC, Buckle T, Bendle G et al (2011) Tracer-cocktail injections for combined pre- and intraoperative multimodal imaging of lymph nodes in a spontaneous mouse prostate tumor model. J Biomed Opt. https://doi.org/10.1117/1.3528027
44. Hekman MCH, Rijpkema M, Bos D et al (2017) Detection of micrometastases using SPECT/fluorescence dual-modality imaging in a CEA-expressing tumor model. J Nucl Med 58:706–710. https://doi.org/10.2967/jnumed.116.185470